RSC Advances

PAPER

View Article Online
View Journal | View Issue

Cite this: *RSC Adv.*, 2021, **11**, 6022

Microstructure design of polypropylene/expandable graphite flame retardant composites toughened by the polyolefin elastomer for enhancing its mechanical properties

Ruilong Li,[ab] Na Wang,[a] Zhuyu Bai,[a] Shaopeng Chen,[a] Jianbing Guo[cd] and Xiaolang Chen *[ac]

The enhanced toughness of flame-retardant polymer composites is still a big challenge due to the deterioration of their mechanical properties. In this work, polypropylene (PP)/nanohybrid expandable graphite (nEG) flame-retardant composites toughened by octene–ethylene copolymer (POE) were fabricated for obtaining good mechanical properties and flame retardancy. The structure, rheological and crystallization behaviors, morphology, flame retardancy, and mechanical property of PP/nEG/POE composites with different contents of POE were investigated. Results show that the elongation at break and impact strength of PP composites were significantly improved due to the incorporation of POE. The elongation at break and notched impact strength of toughened PP composites with only 20% POE were increased to 521.6% and 22.9 kJ m^{-2} from 16.1% and 9.3 kJ m^{-2} for untoughened PP composites, respectively. The scanning electron micrography (SEM) images showed that POE droplets were dispersed finely and uniformly in the PP matrix, exhibiting a typical two-phase structure. Additionally, the interfacial adhesion between the matrix and inorganic particles was enhanced due to the addition of POE. The rheological behaviors of PP composites showed improved elasticity and longer relaxation times, and a stress-yield behavior appeared with the addition of POE. The interfacial interaction in PP composites was enhanced and the formation of an interparticle network was further proved. Additionally, the toughened PP/nEG20 composites with different contents of POE exhibited excellent flame retardancy. Therefore, the toughened flame-retardant PP composites should possess a wider range of application potential.

Received 25th November 2020
Accepted 18th January 2021

DOI: 10.1039/d0ra09978c

rsc.li/rsc-advances

1. Introduction

Polypropylene (PP) is a typical common thermoplastic with high yield, wide application, and low price.[1–3] It has excellent electrical insulation, chemical resistance, and processability.[4,5] However like most polymers, polypropylene has two fatal shortcomings: it is flammable and brittle. The limiting oxygen index (LOI) of PP is only 17.4%. Therefore, flame-retardant[6,7] and toughening[8–11] modification of PP is usually required to expand its application field. In order to improve the flame retardancy and maximize its performance, many studies have been reported for flame-retardant PP composites in recent years.[12–14] On the basis of halogen-free environment protection, one relatively effective method to improve the flame retardancy is to introduce intumescent flame retardants (IFRs) into the PP matrix.[15–18]

Expandable graphite (EG) has been widely used in flame-retardant polymer materials.[19–23] Compared with traditional halogen-free flame retardants, EG is regarded as a new type of IFR because of its outstanding and highly effective flame retardancy. However, EG also has some shortcomings. On the one hand, a "popcorn effect" caused by the combustion process generates a large amount of expandable charred layers, and the interaction between charred layers and the substrate is very weak, and can be easily destroyed. This leads to a poor smoke suppression effect and the generation of droplets. On the other hand, EG particles are easy to agglomerate in the polymer matrix, and the interfacial compatibility is very poor between EG and the polymer, resulting in an outstanding decrease in the mechanical properties of the polymer.[24] Therefore, in order to overcome these problems, it is necessary to modify EG or use EG in conjunction with other additives. Chiang *et al.*[25] reported that

[a]*Key Laboratory of Advanced Materials Technology Ministry of Education, School of Materials Science and Engineering, Southwest Jiaotong University, Chengdu 610031, China. E-mail: chenxl612@sina.com*

[b]*Coal Chemical Industry Technology Research Institute, Ningxia Coal Industry Co. Ltd, China Energy Group, Yinchuan 750411, China*

[c]*Sichuan Jiahe Copoly Technology Co., Ltd., Chengdu 610015, China*

[d]*National Engineering Research Center for Compounding and Modification of Polymer Materials, Guiyang 550014, China*

micro-encapsulated EG obtained by functionalization of the coupling agent has obvious expandability and adhesion, therefore, the interface force between EG and epoxy resin is significantly enhanced. Additionally, composites with excellent mechanical properties and flame retardancy could be obtained. Some investigations have concluded that the particle sizes and expansion of EG has a big effect on the flame retardancy and mechanical properties of polymer matrix composites.[26,27] It was found that the mechanical properties of the composites can be enhanced by decreasing the particle size of EG. However, the expansion volume and flame-retardant efficiency of EG will decrease with decreasing the particle size of EG, which results in a poor flame retardancy of the polymer composites.[26]

Li *et al.*[28] observed an obviously synergistic effect between EG and magnesium hydroxide (MH) in flame-retardant EVA composites. They found that the combination of EG and other additives reduced the total amount of flame retardants for achieving the same flame-retardant level. Xu *et al.*[29] also investigated the influences of the coupling agent on the mechanical properties of PP/EG composites. With regards to the issue of polymer/EG composites, a few ways have been developed, among which microencapsulating EG with the polymer shell was affirmed to be a possible strategy.[30–32] In order to overcome the above shortcomings of EG, functionalized EG wrapped with silica-nanoparticles (nano-SiO_2) were synthesized *via* an *in situ* one-pot method to avoid the popcorn effect of EG and to improve the interfacial adhesion between the polymer and flame retardants.[33] In view of the spherulite structure of PP and taking the chemical groups on the surface of EG into account, nano-SiO_2 was generated on the surface of EG *via* an *in situ* condensation polymerization, where nano-SiO_2 acted as a nucleating agent to improve the interfacial adhesion between EG and PP.

In this study of polymer blends, the addition of thermoplastic elastomers[34] and rubber to toughen plastics represent very important directions.[35] According to the role of the rubber phase in the fracture process of toughened plastics and the energy dissipation path during fracture,[36] several rubber toughening mechanisms have been proposed,[37–39] including the microcrack (craze) mechanism,[40,41] shear craze (shear band) mechanism, void growth mechanism, and local anisotropy. These models consider the respective roles of the rubber phase and matrix phase, and the interaction between the two phases.[42] Elastomer toughening of PP is the most effective toughening method, but it will also reduce the stiffness, strength, and heat resistance of the matrix.[43] In addition, there are common inorganic nanoparticles-toughened PP, such as talcum powder, SiO_2, and $CaCO_3$.[44] The toughened modification of PP/elastomer/inorganic nanoparticles ternary systems has been studied and discussed in detail.[45] The synergistic effect between the added components can greatly improve the toughness of the composites.[46] The effect of the microstructure, phase morphology, and toughening mechanism among the components on their macroscopic properties is complex, but it is a relatively effective method.

In this article, flame-retardant PP composites with octene–ethylene (POE) as a toughening agent and functionalized nanohybrid expandable graphite (nEG) as a high-efficiency flame retardant were prepared by a melt blend. This was expected to further improve the compatibility between PP and nEG. The synergistic effects of nEG and POE particles on the structure, crystallization, and rheological behaviors, phase structure evolution, and mechanical properties of PP/nEG/POE composites were investigated in detail. The purpose of this study was to obtain the best compounding formulation for flame-retardant PP composites with excellent toughness for engineering applications.

2. Experimental

2.1. Materials

Polypropylene (PP, T30S) with a melt flow index (MFI) of 18 g/10 min and a density of 0.92 g cm^{-3} was purchased from Lanzhou Petrochemical, China. The octene–ethylene copolymer (POE, EG8842) was supplied by Dow Chemical Company, USA, with an MFI of 1.0 g/10 min (190 °C/2.16 kg) and density of 0.857 g cm^{-3}. The M_w of POE is 176 900, and the content of octene was 44%. Expandable graphite (EG, C content of 99.6%) with a particle size of 270 μm was supplied by Qingdao Kangboer Graphite Company. Tetraethylorthosilicate (TEOS) and ammonia with a 25% concentration were obtained from Chengdu Kelong Co., Ltd., China. The nanohybrid expandable graphite (nEG) particles were self-prepared in our laboratory according to our previous work.[33]

2.2. Preparation of the PP/nEG/POE composites

The above nEG was dried at 45 °C for 12 h and PP was dried at 80 °C for 6 h. PP, nEG, and POE were pre-mixed at a certain mass ratio and then the mixtures were extruded in a twin-screw extruder at 150 rpm (TSE-20A1600-4-40, Nanjing, China). The temperatures from the hopper to the mold were 170 °C, 180 °C, 190 °C, 205 °C, 210 °C, 210 °C, and 205 °C respectively. The extruded bars were cooled in a water bath and cut into granulates, and then dried in a dryer at 60 °C for 12 h. The dried granulates were injection molded in an injection machine (EM80-V, Cheng De Plastics Machinery) to obtain standard test strips. The formulation of PP composites is presented in Table 1.

2.3. Measurements and characterization

2.3.1. Fourier transform infrared (FTIR) analysis. The FTIR spectra were conducted on a Nicolet 5700 spectrometer (Nicolet Instrument Co., USA) in the wavenumber range of 400–4000 cm^{-1}. Powders of the samples were mixed with KBr powders, and then the mixtures were compressed into plates for FTIR spectral analysis.

2.3.2. X-ray diffraction (XRD) analysis. The XRD patterns of the samples were obtained on an X-ray diffractometer (PANalytical Netherlands), using Cu Kα radiation ($\lambda = 0.15418$ nm) at 40 kV and 20 mA.

2.3.3. Rheological behaviors. The rheological behaviors were assessed on a stress-controlled rheometer (AR1500ex, TA Instruments, USA) in a nitrogen atmosphere. The samples with

Table 1 Formulation and flammability of the PP/nEG20/POE composites with different contents of POE

Samples	PP (%)	nEG (%)	POE (%)	UL-94				LOI (%)
				t_1	t_2	Dripping	Rating	
Pure PP	100	0	0	—	—	Yes	Fail	17.4
PP/nEG20	80	20	0	2.3	2.0	No	V-0	25.4
PP/nEG20/POE5	75	20	5	0	2	No	V-0	22.6
PP/nEG20/POE10	70	20	10	9	2	No	V-0	22.7
PP/nEG20/POE15	65	20	15	0	1	No	V-0	22.8
PP/nEG20/POE20	60	20	20	0	1	No	V-0	22.6

a thickness of 1 mm and diameter of 25 mm were made through compression molding at a melting temperature of 185 °C and pressure of 8 MPa. Frequency sweep tests with an amplitude of 1% were performed in the range of 0.01–100 Hz at a temperature of 185 °C.

2.3.4. Differential scanning calorimetry (DSC) analysis. DSC thermogram analysis was performed under dry nitrogen using a TA instrument Q20 for measuring the nonisothermal crystallization and melting behaviors of the composites. The thermograms were recorded at a heating or cooling rate of 10 °C min^{-1}. The percent crystallinity was determined by dividing the heat of fusion value by 209 J g^{-1}, representing the heat of fusion of 100% crystalline PP.[47]

2.3.5. Polarizing optical microscopy (POM) analysis. POM technology was employed to investigate the crystal morphology of pure PP and its composites with different contents of POE on a CX40P polarizing microscope (Ningbo Shunyu Instrument Co., Ltd., China). The samples were first held in the melt at 230 °C for 5 min and then quickly cooled to 120 °C for 8 h. The overall crystallization behaviors of the samples were also monitored through their digital images.

2.3.6. Scanning electron microscopy (SEM) analysis. The phase morphology and the impact-fractured surface morphology of the samples were characterized by SEM (Model JSM-7500F, Japan) with 20 kV accelerating voltage. In order to characterize the dispersion of POE, the samples were first brittle fractured in liquid nitrogen and then etched in *n*-heptane for 3 h.

2.3.7. Flammability tests. The limited oxygen index (LOI) was surveyed using a JF-4 type instrument (Jiangning Analysis Instrument Factory, China) on 120 × 6.5 × 3.2 mm^3 sheets according to the standard oxygen index test (ASTM D 2863-13). The Underwriters Laboratories-94 (UL-94) vertical burning test was carried out on a CZF-1 type instrument (Jiangning Analytical Instrument Factory, China), with the bar dimensions of 127 × 12.7 × 2.7 mm^3 according to ASTM D3801.

2.3.8. Mechanical properties tests. Tensile strength testing was carried out using a tensile tester (AGS-J) with a crosshead speed of 50 mm min^{-1}. The notched Izod impact was measured on a pendulum impact tester (JBS-300B; Shandong Drick Instruments, China) according to the ASTM D3420 standard. All the tests were performed at 23 ± 2 °C. The results were the average values of at least five specimens.

3. Results and discussion

3.1. Structures of pure PP, PP/nEG20, and PP/nEG20/POE20

The FTIR spectra of pure PP, PP/nEG20 and PP/nEG20/POE20 are shown in Fig. 1. The FTIR spectra shown in Fig. 1 detected the reaction among nEG, PP, and POE. Very strong absorption peaks at 3300–2800 cm^{-1} could be clearly observed for pure PP, which were assigned to CH_3 or CH_2 symmetric and asymmetric vibrations. At the same time, the intensity of the absorption peaks at 3300–2800 cm^{-1} greatly decreased with the incorporation of nEG and POE. However, a wide and strong infrared absorption peak at 3448 cm^{-1} appeared for PP/nEG20

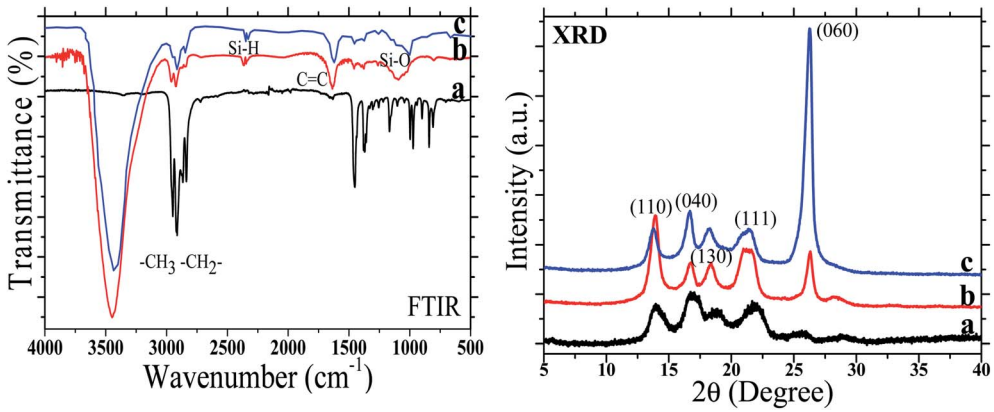

Fig. 1 FTIR spectra and XRD patterns of pure PP and its composites: (a) pure PP; (b) PP/nEG20; (c) PP/nEG20/POE20.

and PP/nEG20/POE20, which belonged to the OH bonds due to the presence of nanohybrid EG and POE. In addition, the introduction of nano-SiO_2 particles in EG also caused the appearance of Si–H and Si–O bonds in PP/nEG20 and PP/nEG20/POE20. Further, the peak of the Si–O bond was shifted to a lower wavenumber due to the interfacial reaction of nEG and POE. All the changes in intensity and position of the absorption peaks revealed the occurrence of the interactions between graphite layers and polymer matrix due to the reaction of POE and nano-SiO_2 particles.

The structural phases of pure PP, PP/nEG20, and PP/nEG20/POE20 were identified by XRD, and the XRD patterns are also plotted in Fig. 1. It was found that there were five main characteristic diffraction peaks of PP at $2\theta = 14.0°$, 16.8°, 18.5°, 21.4°, and 26.2°, which corresponded to the (110), (040), (130), (111), and (060) crystal planes, respectively. For PP/nEG20 and PP/nEG20/POE20 composites, the position of the diffraction peaks remained basically unchanged, indicating that the addition of nEG and POE did not change the crystal structure of PP. However, the width and intensity of these diffraction peaks greatly changed, which may be attributed to the strong reaction of the EG and POE particles. Compared with POE, nEG has better a heterogeneous nucleation effect on PP. Moreover, nEG prevents the induction of POE on β-PP while inducing PP to form α-PP. In addition, most of the diffraction peaks of the PP/nEG20/POE blends were weakened after cross-linking modification, which may be due to the heterogeneous nucleation of branched or cross-linked SiO_2 nanoparticles on PP.

3.2. Rheological performance of pure PP and its composites

The viscosity of a fluid is an expression of the internal friction and a reflection of its resistance to flow. The linear viscoelastic

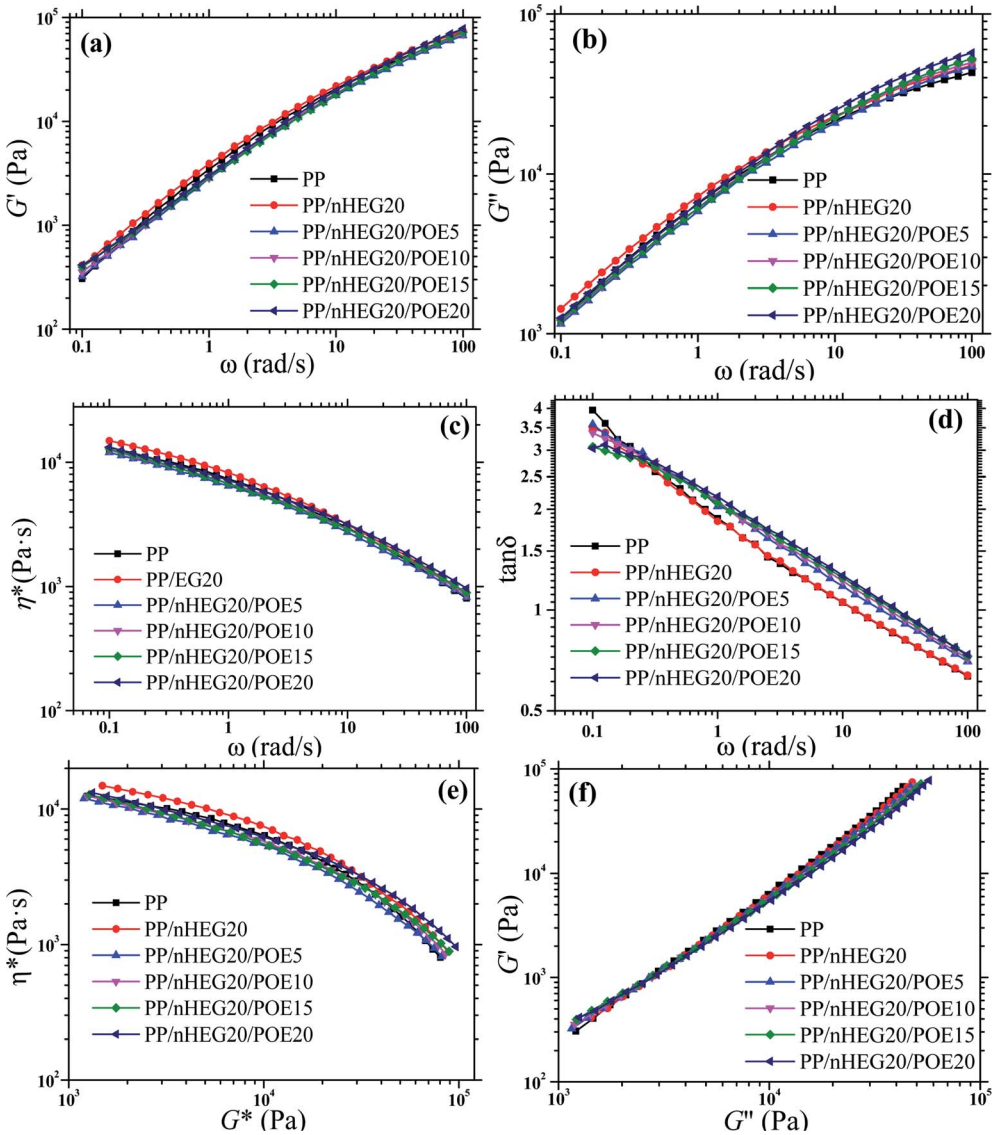

Fig. 2 Linear viscoelastic behaviors of PP and PP/nEG20/POE composites with different contents of POE at 185 °C: (a) storage modulus (G'); (b) loss modulus (G''); (c) complex viscosity (η^*); (d) loss tangent (tan δ); and (e) η^* *versus* complex modulus (G^*); (f) G' *versus* G''.

behaviors of PP and PP/nEG20/POE composites with different contents of POE at 185 °C are shown in Fig. 2. It can be observed from Fig. 2a and b that the values of the storage modulus (G') and loss modulus (G'') for PP and its composites with different contents of POE increased with increasing ω. Compared with pure PP, PP/nEG20 moved up in the whole frequency range, indicating that the melting elasticity had increased and the relaxation time was prolonged. In addition, as the content of POE increased, it had no significant effect on the change of G' and G'' at low frequency. However, the values of G'' showed a slight increase with increasing the POE content at high frequency. This is because the addition of POE increases the deformation resistance of PP/POE blends under external forces.

It can be clearly found from Fig. 2c that all the samples presented higher complex viscosity (η^*) values at low angular frequency than at the high-frequency range. The η^* value of PP and its composites decreased gradually with increasing ω, exhibiting the shear-thinning behavior of a pseudoplastic liquid due to the decrease in the entanglement deformation of the entanglement network. At the same time, the η^* value of PP/nEG20 was higher than that of the PP and PP/nEG20/POE composites. Because nEG is a solid particle, so more free volumes will be occupied between the molecular chains, and the moving units of the molecular chains also will be decreased, making the fluidity worse and resulting in a deterioration of the flexibility of the composites, which in turn increases the η^* of the materials at low frequency. With the addition of POE, the η^* values of PP/nEG20/POE composites decreased. Also, η^* showed a slight upward trend with increasing the content of POE. At the low-frequency region, although η^* varied with increasing the POE content, this was relatively slow. At the high-frequency region, the effect was much more sensitive and even upturned. This also balances the influence of nEG and elastomer on the η^* of the composites, which is beneficial to the processing of the composites.

The loss tangent (tan δ) curves of PP and its composites as a function of ω are plotted in Fig. 2d. The tan δ values can well show the viscoelasticity of the samples. Compared with pure PP, the tan δ value of PP/nEG20 only decreased slightly at the low-frequency region, and there was almost no change at the high-frequency region. However, the tan δ value of PP/nEG20/POE composites was greatly affected by POE. The tan δ value of the composites at the low-frequency region was lower than that of PP and higher than that of PP at the high-frequency region. This indicates that the PP composites with POE exhibited elasticity at the low-frequency region and mainly exhibited viscosity at the high-frequency region.

Table 2 DSC data of PP/nEG20 and PP/nEG20/POE composites with different contents of POE

Samples	T_m (°C)	T_c (°C)	ΔH_m (J g^{-1})	ΔH_c (J g^{-1})	X_c (%)
Pure PP	161.6	113.7	99.9	123.4	47.8
PP/nEG20	163.7	125.6	86.0	100.8	51.4
PP/nEG20/POE5	163.3	122.3	84.9	94.0	54.2
PP/nEG20/POE10	163.3	123.5	52.1	58.3	35.6
PP/nEG20/POE15	163.3	123.2	44.9	52.6	33.1
PP/nEG20/POE20	163.1	122.5	35.2	50.0	28.1

The stress-yielding behaviors of the samples can be seen by the relationship between η^* and complex modulus (G^*), as shown in Fig. 2e. This behavior is mainly manifested in incompatible blends and filling systems of inorganic particles. If η^* suddenly appears upturned at the low G^* interval, it indicates that the sample has a stress-yield behavior. In the case of PP, at the low G^* interval, the η^* gradually approached a plateau, exhibiting Newtonian fluid behaviors. Compared with pure PP, PP/nEG20 appeared to be warping at the low G^* range. The upward warping phenomenon became slow with the addition of POE. However, with increasing the POE content, the phenomenon of warping at the low G^* region became obvious, which indicated that the PP composites with POE had obvious stress-yielding behaviors.

The Han curve is the lg G' − lg G'' curve for homopolymers based on the molecular viscoelasticity theory of monodisperse and polydisperse homopolymers that was first reported in 1982. The Han curves of PP and its composites are exhibited in Fig. 2f. No major change in the Han curves of PP and PP/nEG20 could be observed. Both slopes slightly decreased at the low G'' region, and were uplifted at the high G'' region, showing good elastic

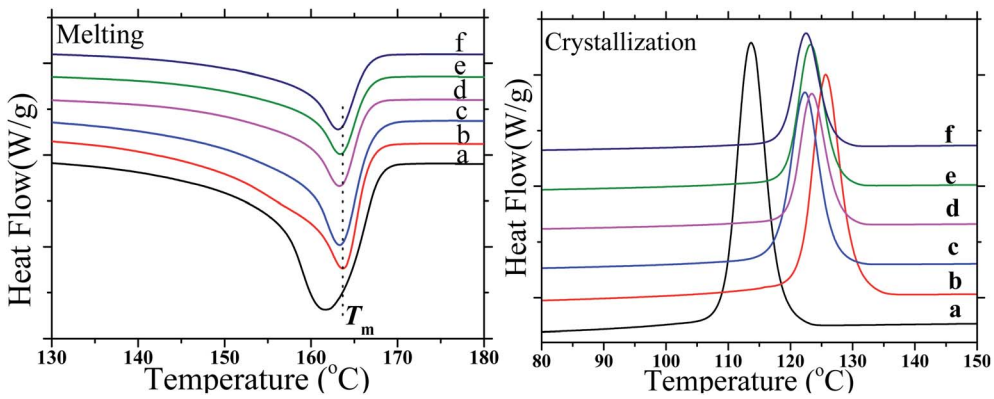

Fig. 3 DSC melting and crystallization curves of pure PP and PP/nEG20/POE composites with different contents of POE: (a) pure PP; (b) 0 wt%; (c) 5 wt%; (d) 10 wt%; (e) 15 wt%; and (f) 20 wt%.

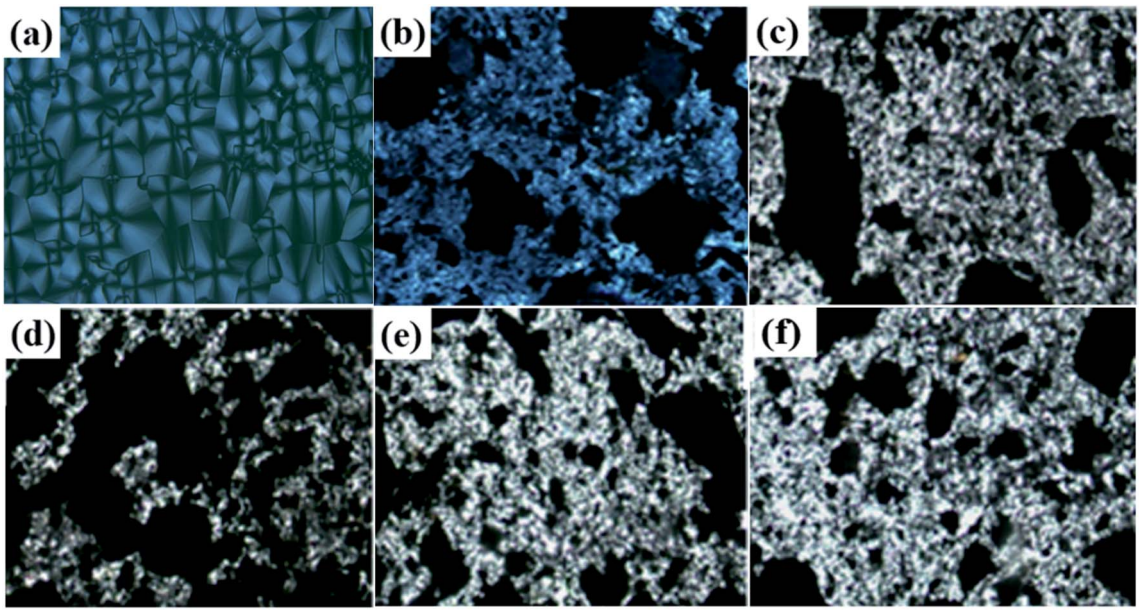

Fig. 4 Crystal morphology of pure PP and PP/nEG20/POE composites with different contents of POE at 120 °C for 8 h: (a) pure PP; (b) 0 wt%; (c) 5 wt%; (d) 10 wt%; (e) 15 wt%; and (f) 20 wt%.

behaviors. With the addition of POE, there was a slight decrease at the high G'' region compared to pure PP and PP/nEG20. Also, with increasing the content of POE elastomer, the decline phenomenon was more obvious. This indicated that the addition of POE changed the processing behaviors of the composites.

3.3. Melting and crystallization behaviors of pure PP and its composites

The DSC melting and crystallization behaviors of pure PP and PP/nEG20/POE composites with different contents of POE are shown in Fig. 3, and the corresponding data are listed in Table 2. It can be clearly found from Fig. 3 that nEG and POE had a great effect on the melting and crystallization behaviors of the PP matrix. Additionally, only a single melting and crystallization peak for all the samples was observed in the DSC curves. The melting temperature (T_m) and crystallization temperature (T_c) of PP were 164.1 °C and 113.7 °C, respectively. With the addition of 20% nEG, the T_m and T_c values of the PP/nEG20 composites increased. This indicated that the thermal property of PP was enhanced slightly, and nEG had a heterogeneous nucleation effect on the PP matrix. On the other hand, the addition of POE

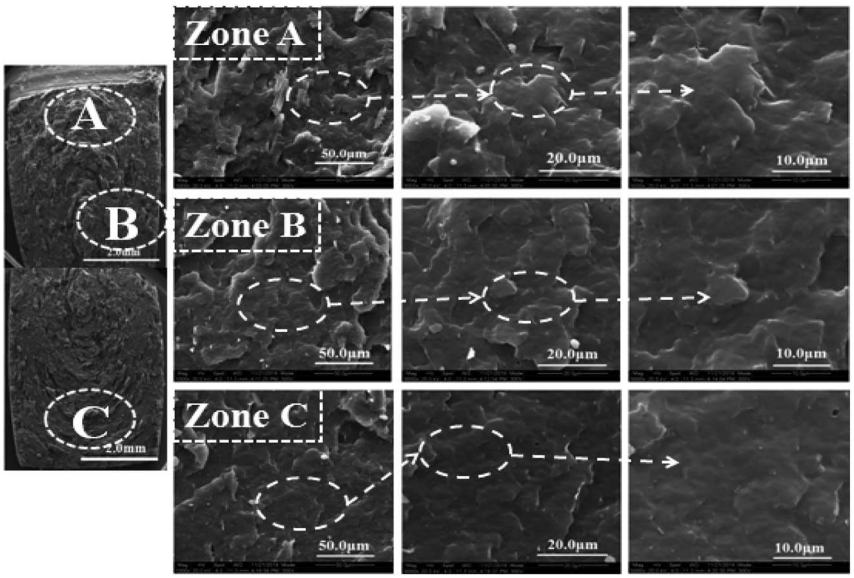

Fig. 5 SEM images of the impact-fractured surface morphologies of PP/nEG20 composites.

had little effect on the T_m of the samples. However, the T_c values of the PP/nEG20/POE composites decreased slightly with the addition of POE compared with the PP/nEG20 composites. This indicated that the incorporation of POE weakened the heterogeneous nucleation effect of nEG on PP.

In addition, when 20% nEG was added into PP matrix, the crystallinity (X_c) of the PP/nEG20 composites was also improved compared with pure PP. Because of the heterogeneous nucleation of nEG, the crystallization process of PP was accelerated, and the X_c value of the PP/nEG20 composites increased. However, with the addition of 5 wt% POE, the X_c value of the PP/nEG20/POE composites increased further, which was attributed to the improved uniform dispersion of nEG in the matrix. However, with increasing the content of POE, the X_c value of the PP/nEG20/POE composites decreased quickly. Because the excessive POE intertwined with the molecular chains of PP, which hindered the diffusion of the molecular chains of PP into the crystal lattice, it was difficult for PP to crystallize. This is also the reason why the crystallinity first increased and then decreased as the POE content increased.

It is of great significance to study the structure, formation conditions, influencing factors, and deformation and failure of spherulites. The crystal morphologies of pure PP and its composites at 120 °C for 8 h are shown in Fig. 4. For pure PP, the spherulite structure was dense and complete, and the interface between spherulites was very clear. In addition, the density of spherulite was large, as shown in Fig. 4a. When 20% nEG particles was added into the PP matrix, it could be observed from Fig. 4b that the heterogeneous nucleation of nEG on PP caused the crystals to become smaller, which successfully regulated the grain size of PP. At the same time, the interaction between inorganic particles and PP molecular chains limited the movement of PP molecular chains, resulting in a more incomplete crystallization of PP. With the addition of POE, the distribution of nEG in the polymer matrix became more uniform, resulting in the stress field around the elastomer being easier to generate. Also, the distribution of voids was more dispersed, as shown in Fig. 4c–f. The POE and the PP molecular chains were entangled with each other, so that the rearrangement movement of the PP molecular chain occurred during the crystallization process. Additionally, the presence of POE limited the effect of nEG on the crystallization of PP. The introduction of POE had no further effect on the grain size of the matrix, but excessive POE restricted the diffusion and accumulation of PP chains into the crystal lattice, making crystallization difficult. This also explains the change in crystallinity mentioned in the DSC section above.

3.4. Flammability of pure PP and its composites

The UL-94 and LOI results of pure PP and PP/nEG20/POE composites with various contents of POE are listed in Table 1. It can be seen from Table 1 that the LOI values of pure PP and PP/nEG20 composite were 17.4% and 25.4%, respectively. With the addition of POE, the LOI value of the composites decreased slightly because of the flammability of POE, but the UL-94 grade did not decrease. All the samples could reach the UL-94 V-0 level. This indicates that the incorporation of POE had little effect on the vertical combustion result of the composites, and the composites achieved a good flame retardancy.

3.5. Morphology analysis of the PP composites

The mechanical properties of polymer composites are greatly affected by the morphological structure constructed during processing.[48] In this work, in order to analyze to relationship between the mechanical property and morphological structure, SEM analysis was carried out to investigate the morphological structures of the PP/nEG20 and PP/nEG20/POE composites. Fig. 5–9 show the morphologies of the PP/nEG20 and PP/nEG20/POE composites with different proportions of POE, respectively. It can be observed from Fig. 5 that nanohybrid EG particles were uniformly dispersed in the PP matrix, and almost no debonding

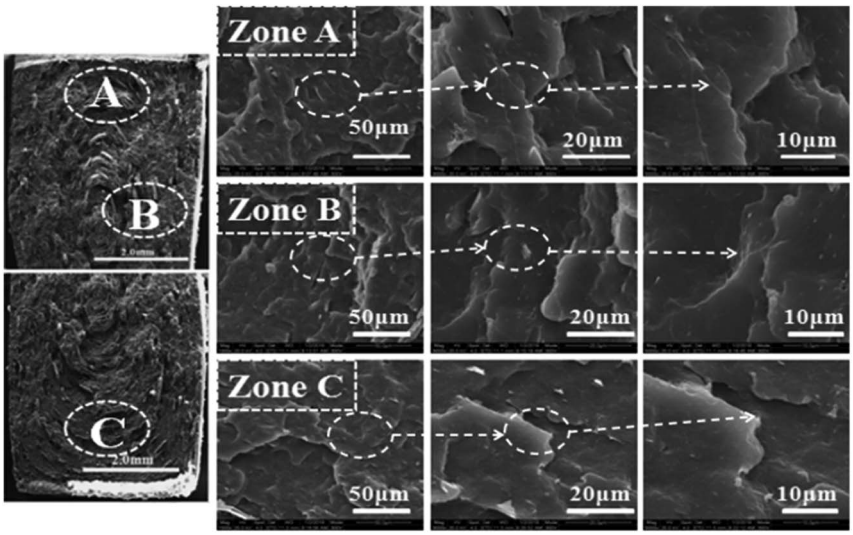

Fig. 6 SEM images of the impact-fractured surface morphologies of PP/nEG20/POE composites with 5 wt% POE.

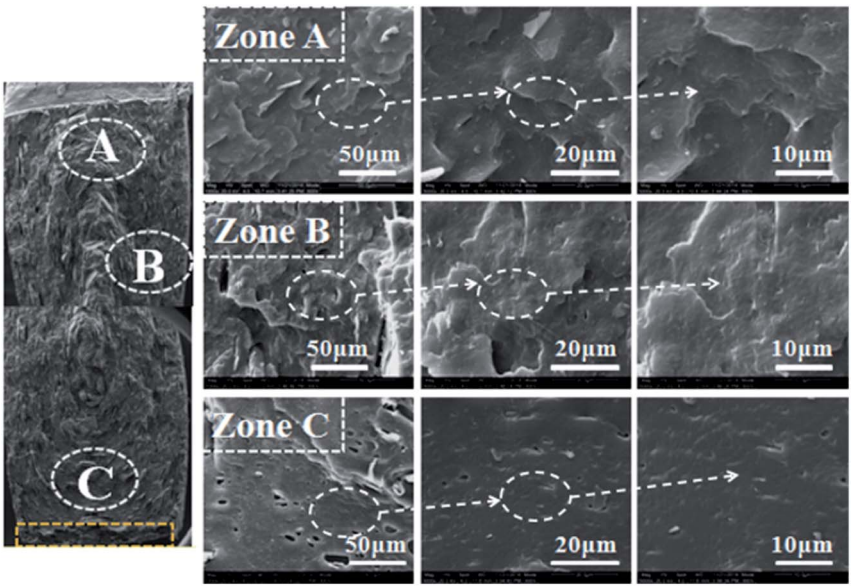

Fig. 7 SEM images of the impact-fractured surface morphologies of PP/nEG20/POE composites with 10 wt% POE.

could be observed at the interfaces between PP and EG. However, the interfacial adhesion of PP and EG was enhanced by nano-SiO_2 particles, and the fracture section of the PP/nEG20 composites was very rough. This reveals a better wetting of nEG particles with the PP matrix. On the other hand, the addition of POE had an obvious influence on the fractured morphology of PP/nEG20/POE composites, as shown in Fig. 6–9. The PP composites with various POE contents still had wetting of the dispersed phase in the PP matrix. The nEG particles and POE were uniformly dispersed in the PP matrix. In addition, an obscure boundary between two phases could be clearly found, and a more deformed polymer structure could be observed at the interfaces with increasing the content of POE. This suggests that the interfacial adhesion was enhanced significantly, resulting in the high impact strength and elongation at break for the PP/nEG20/POE composites with a high content of POE.

To further investigate the phase morphology and dispersion analysis of PP/nEG20/POE with different contents of POE, the samples were freeze-fractured in liquid nitrogen for 30 min and then selectively etched in *n*-heptane for 3 h to remove the POE phase, and the results are shown in Fig. 10. It can be found from Fig. 10a that the surface of PP/nEG20 was not changed, and the interface compatibility between nEG and PP was good. With the addition of POE, graphite-sized holes appeared on the freeze-fractured surface due to the removal of POE domains. It is known that POE was also scattered on the interface between

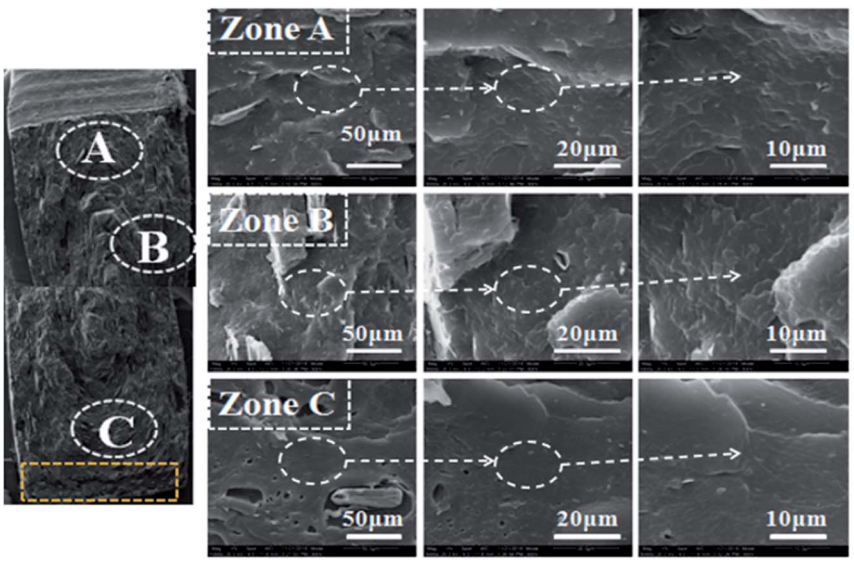

Fig. 8 SEM images of the impact-fractured surface morphologies of PP/nEG20/POE composites with 15 wt% POE.

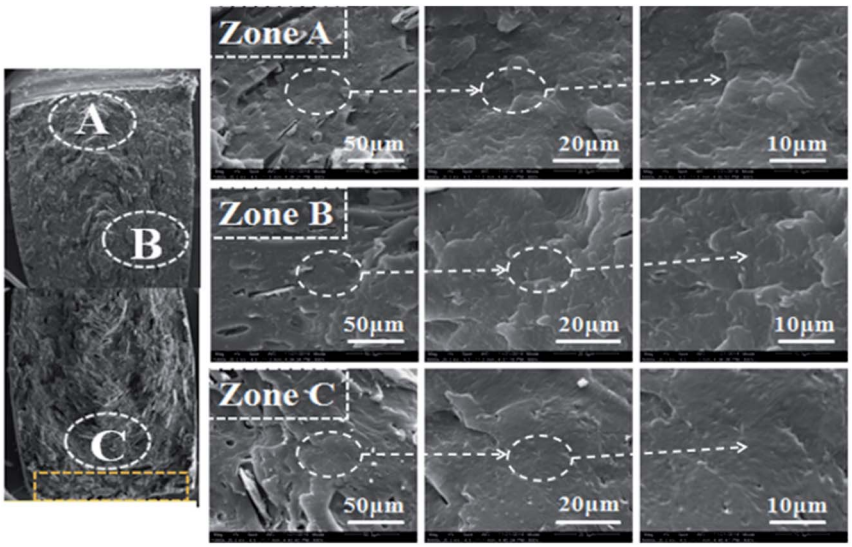

Fig. 9 SEM images of the impact-fractured surface morphologies of PP/nEG20/POE composites with 20 wt% POE.

nEG and PP, as shown in Fig. 10b–e. Also, an obvious "sea-island" structure can be clearly observed. With increasing the content of POE, more and more spherical voids were formed, which were generated after the *n*-heptane etching of POE. However, the particle size of the void did not change. The SEM images showed a clear two-phase morphology for all the composites with different contents of POE, and the droplets of POE particles were uniformly dispersed in the polymer matrix. This is responsible for the improved toughness of the composites.

3.6. Mechanical property of pure PP and its composites

Fig. 11 shows the typical tensile stress–strain curves of the PP-based flame-retardant composites with different contents of POE, and the corresponding results and impact strength are listed in Table 3. It can be concluded from Table 3 that the notched impact strength of pure PP was only 6.6 kJ m^{-2}. The impact strength of PP/nEG20 composites with 20 wt% nEG increased to 9.3 kJ m^{-2}, which is attributed to the improved interfacial adhesion and compatibility caused by the nano-hybrid. On the other hand, when POE was incorporated into the composites, the impact strength of the PP/nEG20/POE composites increased rapidly with increasing the content of POE. For example, the impact strength of the composites was 10.4 kJ m^{-2} at a POE content of 5 wt%; however, the impact strength of the PP/nEG20/POE20 composites with 20 wt% POE was increased to 22.5 kJ m^{-2}. These results imply that the toughening effect of POE on the PP-based composites was highly outstanding.

It can be found from Fig. 11 and Table 3 that the elongation at break of the PP/nEG20 composites decreased dramatically when 20wt% nEG was added into the PP matrix. However, for

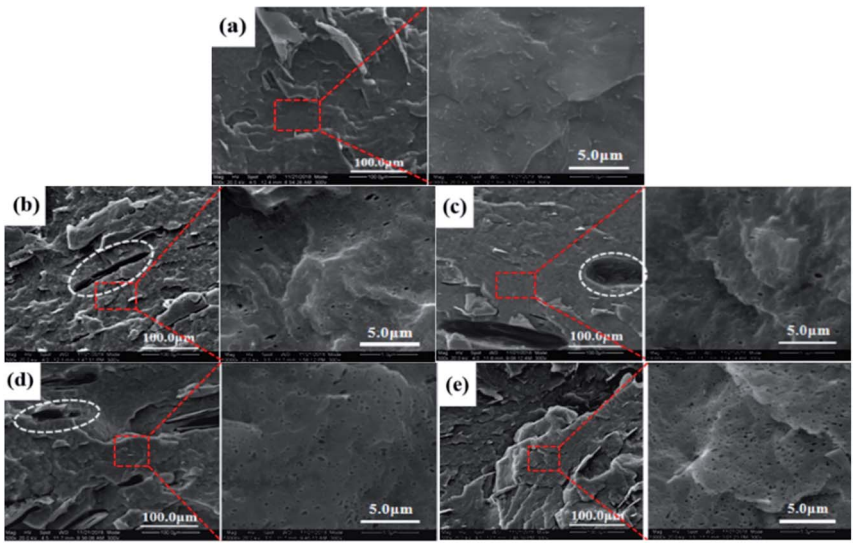

Fig. 10 Dispersion of POE in the PP/nEG20/POE composites with different contents of POE: (a) 0 wt%; (b) 5 wt%; (c) 10 wt%; (d) 15 wt%; and (e) 20 wt%.

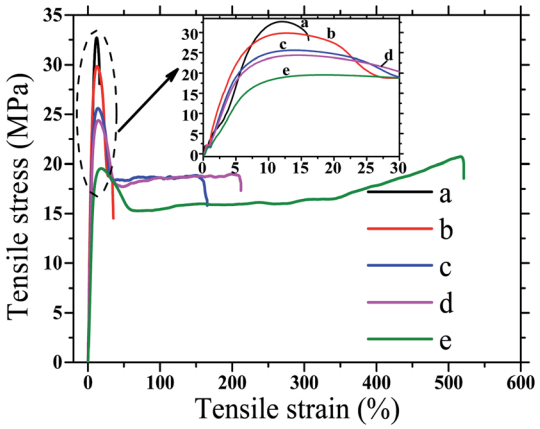

Fig. 11 Tensile stress *versus* strain curves of PP/nEG20/POE composites with different contents of POE: (a) 0 wt%; (b) 5 wt%; (c) 10 wt%; (d) 15 wt%; and (e) 20 wt%.

Table 3 Mechanical properties of PP/nEG20 and PP/nEG20/POE composites with different contents of POE

Samples	Tensile strength (MPa)	Elongation at break (%)	Impact strength (kJ m^{-2})
Pure PP	33.1 ± 0.5	706.7 ± 10	6.6 ± 0.2
PP/nEG20	32.7 ± 0.4	16.1 ± 2	9.3 ± 0.2
PP/nEG20/POE5	30.0 ± 0.3	35.2 ± 3	10.4 ± 0.3
PP/nEG20/POE10	25.7 ± 0.3	166.5 ± 5	13.8 ± 0.2
PP/nEG20/POE15	24.5 ± 0.3	212.2 ± 8	17.2 ± 0.3
PP/nEG20/POE20	19.7 ± 0.2	521.6 ± 9	22.9 ± 0.3

the PP/nEG20/POE composites with different contents of POE, the elongation at break increased sharply with increasing the content of POE. The toughness expressed as the work to fracture (the area under the stress–strain curve) was consistent with the result of the elongation at break. However, it seems that the tensile strength tended to decrease with increasing the content of POE. These results reveal that the interaction and interfacial adhesion between the polymer and inorganic particles were enhanced due to the incorporation of POE. The elongation at break and impact strength for the PP-based composites with different contents of POE were excellent. Therefore, the improvement of the mechanical properties can be ascribed to the incorporation of the third component. It seems that POE had a synergistic toughening effect with nanohybrid EG on the PP matrix. Accordingly, the proposed mechanism of the enhanced compatibility for POE-toughened PP/nEG composites is illustrated in Fig. 12. Therefore, the combination of POE and nEG is regarded as a good way to enhance the tensile strength and toughness of PP composites.

4. Conclusions

In this work, octene–ethylene (POE) was used as a toughening agent to toughen PP/nEG20 composites to fabricate high-impact PP-based flame-retardant composites. The structure, rheological and crystallization behaviors, phase morphology, flame retardancy, and mechanical property of the PP/nEG/POE composites with different contents of POE were assessed. It was found that POE had little effect on the structure of the composites. In addition, the crystallization behavior and crystal morphology of the PP composites were greatly affected by nEG and POE. The addition of POE improved the elasticity of the composites, making the composites exhibit a longer relaxation time and stress-yielding behaviors. The PP-based composites with different contents of POE retained good flame retardancy. Finally, it is concluded that the combination

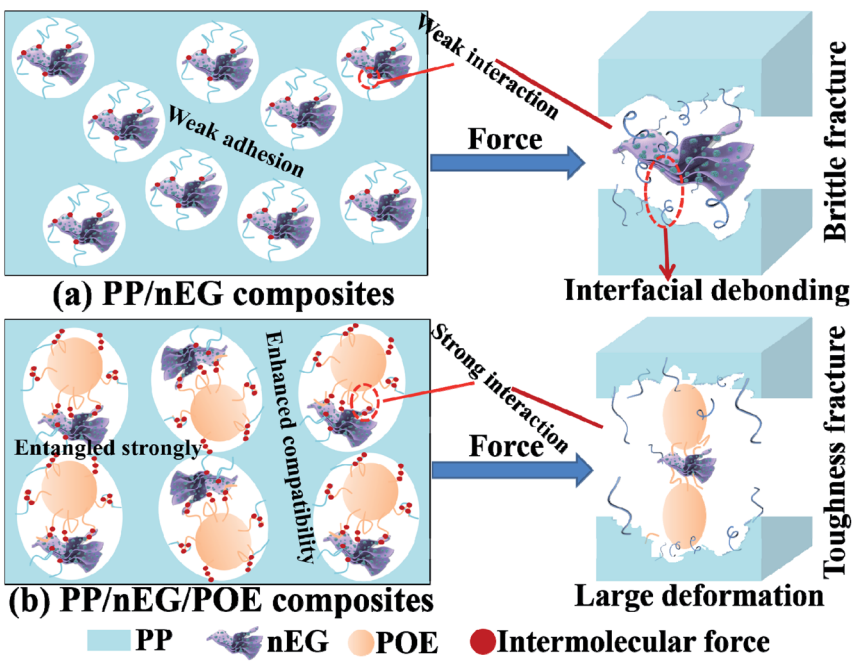

Fig. 12 Schematic diagram for the compatibility enhancement of graphite layers with the PP matrix.

of nanohybrid EG and POE exhibited outstanding mechanical performances, especially an excellent elongation at break and notched impact strength. This can be attributed to the synergistic toughening effect of nanohybrid and POE on the PP-based composites. This work proposes an efficient way to toughen PP-based flame-retardant composites by using the synergistic effect of nanohybrid particles and POE, which can be widely applied in many fields.

Conflicts of interest

The authors declared that they have no conflicts of interest to this work. We declare that we do not have any commercial or associative interest that represents a conflict of interest in connection with the work submitted.

Acknowledgements

This work was financially supported by the National Natural Science Foundation of China (51763002), Opening Project of State Key Laboratory of Polymer Materials Engineering (Sichuan University) (sklpme2020-4-01), International Science and Technology Cooperation Project of Chengdu (2020-GH02-00010-HZ, 2019-GH02-00026-HZ), Science and Technology Talent Innovation and Entrepreneurship Project of Chengdu (2020-GH02-00010-HZ), Science Research Project of Guizhou Department of Education ([2019]068), and High-level Innovative Talent-training Program in Guizhou ([2016]5667).

References

1 X. S. Li, Z. L. Zhao, Y. H. Wang, H. Yan and B. S. Xu, Highly efficient flame retardant, flexible, and strong adhesive intumescent coating on polypropylene using hyperbranched polyamide, *Chem. Eng. J.*, 2017, **324**, 237–250.

2 Q. H. Kong, T. Wu, H. K. Zhang, Y. Zhang, M. M. Zhang, T. Y. Si, L. Yang and J. H. Zhang, Improving flame retardancy of IFR/PP composites through the synergistic effect of organic montmorillonite intercalation cobalt hydroxides modified by acidified chitosan, *Appl. Clay Sci.*, 2017, **146**, 230–237.

3 J. X. Zhu, Y. L. Zhu, W. X. Song, H. Wang, M. Gao, M. Cho and I. Park, Zinc oxide enhanced piezoelectret polypropylene microfiber for mechanical energy harvesting, *ACS Appl. Mater. Interfaces*, 2018, **10**, 19940–19947.

4 S. B. Nie, L. Liu, G. L. Dai and C. Zhou, Investigation on pyrolysis of intumescent flame-retardant polypropylene (PP) composites based on synchrotron vacuum ultraviolet photoionization combined with molecular-beam mass spectrometry, *J. Therm. Anal. Calorim.*, 2017, **130**, 1003–1009.

5 L. J. Han, W. H. Wu, Y. X. Qi, H. Q. Qu and J. Z. Xu, Synergistic flame retardant effect of $BiFeO_3$ in intumescent flame-retardant polypropylene composites, *Polym. Compos.*, 2017, **38**, 2771–2778.

6 L. G. Lu, N. Guo, X. D. Qian, S. S. Yang and G. S. Shao, Thermal degradation and combustion behavior of intumescent flame-retardant polypropylene with novel phosphorus-based flame retardants, *J. Appl. Polym. Sci.*, 2018, **135**, 45962–45971.

7 C. J. Zhu, M. S. He, Y. Liu, J. G. Cui, Q. L. Tai, L. Song and Y. Hu, Synthesis and application of a mono-component intumescent flame retardant for polypropylene, *Polym. Degrad. Stab.*, 2018, **151**, 144–151.

8 G. Y. Liu and G. X. Qiu, Study on the mechanical and morphological properties of toughened polypropylene blends for automobile bumpers, *Polym. Bull.*, 2013, **70**, 849–857.

9 S. Houshyar and R. A. Shanks, Mechanical and thermal properties of toughened polypropylene composites, *J. Appl. Polym. Sci.*, 2010, **105**, 390–397.

10 X. L. Chen, J. Yu, Z. Luo, S. Y. Guo, M. He and Z. W. Zhou, Study on mechanical properties and phase morphology of polypropylene/polyolefin elastomer/magnesium hydroxide ternary composites, *Polym. Adv. Technol.*, 2011, **22**, 657–663.

11 H. J. Zhang, J. W. Wang, S. K. Cao and Y. Wang, Toughened polypropylene with balanced rigidity. IV. Morphology, crystallization behavior, and thermal properties, *J. Appl. Polym. Sci.*, 2001, **79**, 1351–1358.

12 H. J. Lin, H. Yan, B. Liu, L. Q. Wei and B. S. Xu, The influence of KH-550 on properties of ammonium polyphosphate and polypropylene flame retardant composites, *Polym. Degrad. Stab.*, 2011, **96**, 1382–1388.

13 Z. H. Zheng, Y. Liu, L. Zhang and H. Y. Wang, Synergistic effect of expandable graphite and intumescent flame retardants on the flame retardancy and thermal stability of polypropylene, *J. Mater. Sci.*, 2016, **51**, 5857–5871.

14 L. Ballice and R. Reimert, Classification of volatile products from the temperature-programmed pyrolysis of polypropylene (PP), atactic-polypropylene (APP) and thermogravimetrically derived kinetics of pyrolysis, *Chem. Eng. Process.*, 2002, **41**, 289–296.

15 J. F. Wang, X. X. Jin, C. H. Li, W. J. Wang, H. Wu and S. Y. Guo, Graphene and graphene derivatives toughening polymers: toward high toughness and strength, *Chem. Eng. J.*, 2019, **370**, 831–854.

16 X. J. Lai, X. R. Zeng, H. Q. Li, F. Liao, H. L. Zhang and C. Y. Yin, Synergistic effect of phosphorus-containing montmorillonite with intumescent flame retardant in polypropylene, *J. Macromol. Sci., Part B: Phys.*, 2012, **51**, 1186–1198.

17 M. Thirumal, Recent developments of intumescent fire protection coatings for structural steel: a review, *J. Fire Sci.*, 2016, **34**, 120–163.

18 H. J. Duan, H. Q. Kang, W. Q. Zhang, X. Ji, Z. M. Li and J. H. Tang, Core-shell structure design of pulverized expandable graphite particles and their application in flame-retardant rigid polyurethane foams, *Polym. Int.*, 2014, **63**, 72–83.

19 F. Qi, M. Q. Tang, N. Wang, N. Liu, X. L. Chen, Z. B. Zhang, K. Zhang and X. Lu, Efficient organic-inorganic intumescent interfacial flame retardants to prepare flame retarded

polypropylene with excellent performance, *RSC Adv.*, 2017, **7**, 31696–31706.

20 H. J. Kruger, W. Focke, W. Mhike and A. Taute, Thermal properties of polyethylene flame retarded with expandable graphite and intumescent fire retardant additives, *Fire Mater.*, 2017, **41**, 573–586.

21 X. Han, T. B. Zhao, X. Gao and H. Y. Li, Preparation and characterization of high-temperature non-flowing SiO2/EG/paraffin composites by high-temperature refining, *Colloids Surf., A*, 2018, **542**, 1–7.

22 T. Guler, U. Tayfun, E. Bayramli and M. Dogan, Effect of expandable graphite on flame retardant, thermal and mechanical properties of thermoplastic polyurethane composites filled with huntite and hydromagnesite mineral, *Thermochim. Acta*, 2017, **647**, 70–80.

23 L. J. Li, Y. J. Chen, L. J. Qian, B. Xu and W. Xi, Addition flame retardant effect of nonreactive phosphonate and expandable graphite in rigid polyurethane foams, *J. Appl. Polym. Sci.*, 2018, **135**, 45960–45968.

24 X. L. Zhang, H. J. Duan, D. X. Yan, L. Q. Kang, W. Q. Zhang and J. H. Tang, A facile strategy to fabricate microencapsulated expandable graphite as a flame-retardant for rigid polyurethane foams, *J. Appl. Polym. Sci.*, 2015, **132**, 42364–42372.

25 C. L. Chiang and S. W. Hsu, Novel epoxy/expandable graphite halogen-free flame retardant composites-preparation, characterization, and properties, *J. Polym. Res.*, 2010, **17**, 315–323.

26 L. Shi, Z. M. Li, B. H. Xie, J. H. Wang and M. B. Yang, Flame retardancy of different-sized expandable graphite particles for high-density rigid polyurethane foams, *Polym. Int.*, 2010, **55**, 862–871.

27 Z. D. Sun, Y. H. Ma, Y. Xu, X. L. Chen, M. Chen, J. Yu, Z. B. Zhang and S. C. Hu, Effect of the particle size of expandable graphite on the thermal stability, flammability, and mechanical properties of high-density polyethylene/ethylene vinyl-acetate/expandable graphite composites, *Polym. Eng. Sci.*, 2014, **54**, 1162–1169.

28 Z. Z. Li and B. J. Qu, Flammability characterization and synergistic effects of expandable graphite with magnesium hydroxide in halogen-free flame-retardant EVA blends, *Polym. Degrad. Stab.*, 2003, **81**, 401–408.

29 Y. Xu, M. Chen, X. Ning, X. L. Chen, Z. D. Sun, Y. H. Ma, J. Yu, Z. B. Zhang, X. J. Bo, L. Yang and Z. N. Chen, Influences of coupling agent on thermal properties, flammability and mechanical properties of polypropylene/thermoplastic polyurethanes composites filled with expanded graphite, *J. Therm. Anal. Calorim.*, 2014, **115**, 689–695.

30 X. G. Zhang, L. L. Ge, W. Q. Zhang, J. H. Tang, L. Ye and Z. M. Li, Expandable graphite-methyl methacrylate-acrylic acid copolymer composite particles as a flame retardant of rigid polyurethane foam, *J. Appl. Polym. Sci.*, 2011, **122**, 932–941.

31 B. B. Wang, S. Hu, K. M. Zhao, H. D. Lu, L. Song and Y. Hu, Preparation of polyurethane microencapsulated expandable graphite, and its application in ethylene vinyl acetate copolymer containing silica-gel microencapsulated ammonium polyphosphate, *Ind. Eng. Chem. Res.*, 2011, **50**, 11476–11484.

32 J. P. Han, G. Z. Liang, A. J. Gu, J. H. Ye, Z. Y. Zhang and L. Yuan, A novel inorganic-organic hybridized intumescent flame retardant and its super flame retarding cyanate ester resins, *J. Mater. Chem. A*, 2013, **1**, 2169–2182.

33 N. Wang, *Master degree thesis*, Southwest Jiaotong University, 2016.

34 J. H. Lin, Y. J. Pan, C. F. Liu, C. L. Huang, C. T. Hsieh, C. K. Chen, Z. L. Lin and C. W. Lou, Preparation and compatibility evaluation of polypropylene/high density polyethylene polyblends, *Materials*, 2015, **8**, 8850–8862.

35 Y. M. Zeybek and C. Kaynak, Loss of thermoplastic elastomer toughening in polylactide after weathering, *J. Appl. Polym. Sci.*, 2018, **136**, 47177–47188.

36 H. Keskkula, D. R. Paul, K. M. McCreedy and D. E. Henton, Methyl methacrylate grafted rubbers as impact modifiers for styrenic polymers, *Polymer*, 1987, **28**, 2063–2069.

37 A. M. L. Magalhaes and R. J. M. Borggreve, Contribution of the crazing process to the toughness of rubber-modified polystyrene, *Macromolecules*, 1995, **28**, 5841–5851.

38 P. Kannan and M. Sevi, Studies on photocrosslinkable-cum-flame retardant poly (benzylidene phosphoramide ester)s, *J. Polym. Sci., Part A: Polym. Chem.*, 1999, **37**, 3285–3291.

39 R. K. Jian, L. Chen, S. Y. Chen, J. W. Long and Y. Y. Wang, A novel flame-retardant acrylonitrile-butadiene-styrene system based on aluminum isobutylphosphinate and red phosphorus: flame retardance, thermal degradation and pyrolysis behavior, *Polym. Degrad. Stab.*, 2014, **109**, 184–193.

40 C. B. Bucknall, R. Rizzieri and D. R. Moore, Detection of incipient rubber particle cavitation in toughened PMMA using dynamic mechanical tests, *Polymer*, 2000, **41**, 4149–4156.

41 F. Ramsteiner, G. E. Mckee and M. Breulmann, Influence of void formation on impact toughness in rubber modified styrenic-polymers, *Polymer*, 2002, **43**, 5995–6003.

42 J. S. Jayan, A. Saritha and K. Joseph, Innovative materials of this era for toughening the epoxy matrix: a review, *Polym. Compos.*, 2018, **39**, E1959–E1986.

43 J. Banerjee, P. Soliya, M. B. Pallavi, P. Mukhopadhyay, S. Bandyopadhyay, D. Chakrabarty and K. Dutta, Impact Modification of Isotactic Polypropylene with Ethylene-Propylene Diene, *Int. Polym. Process.*, 2016, **31**, 188–197.

44 X. H. Li, Y. D. He, X. F. Li, F. An, D. Z. Yang and Z. Z. Yu, Simultaneous enhancements in toughness and electrical conductivity of polypropylene/carbon nanotube nanocomposites by incorporation of electrically inert calcium carbonate nanoparticles, *Ind. Eng. Chem. Res.*, 2017, **56**, 2783–2788.

45 X. H. Chi, L. Cheng, W. F. Liu, X. H. Zhang and S. T. Li, Characterization of polypropylene modified by blending elastomer and nano-silica, *Materials*, 2018, **11**, 1321.

46 M. Haghnegahdar, G. Naderi and M. H. R. Ghoreishy, Fracture toughness and deformation mechanism of un-vulcanized and dynamically vulcanized polypropylene/

ethylene propylene diene monomer/graphene nanocomposites, *Compos. Sci. Technol.*, 2017, **141**, 83–98.
47 X. L. Chen, J. Yu and S. Y. Guo, Structure and properties of polypropylene composites filled with magnesium hydroxide, *J. Appl. Polym. Sci.*, 2006, **102**, 4943–4951.
48 G. X. Wang, S. Li, Y. L. Feng, Y. X. Hu, G. Y. Zhao and W. Jiang, Effectively toughening polypropylene with in situ formation of core-shell starch-based particles, *Carbohydr. Polym.*, 2020, **249**, 116795.